Improvement of cob thermal inertia by latent heat storage and its implication on energy consumption

Farjallah Alassaad, Karim Touati, Daniel Levacher, Yassine El Mendili, Nassim Sebaibi

Version of Record: https://www.sciencedirect.com/science/article/pii/S0950061822008443
Manuscript_e7dfae40bbce69440ffa6c4e61242a86

Improvement of cob thermal inertia by latent heat storage and its implication on energy consumption

Farjallah Alassaad[1], Karim Touati[1], Daniel Levacher[2], Yassine El Mendili[1], Nassim Sebaibi[1]
[1]COMUE NU, Laboratoire de Recherche, ESITC Caen, 1 Rue Pierre et Marie Curie, 14610 Epron, France
[2]COMUE NU, M2C UMR 6143 CNRS, Université de Caen Normandie, 24 rue des Tilleuls, 14000 Caen, France

Highlights

- Introduction of phase change materials (PCM) into cob.
- Improvement of cob thermal properties with PCMs incorporation.
- Degradation of cob hygroscopic and mechanical properties with PCMs incorporation.
- Reduction of energy consumption in cob house incorporating PCMs in their walls.

Abstract

Climate change imposes new guidelines on our planet. Due to its impact on the environment, construction industry must invest in the development of new building solutions or the improvement of the existing ones. Thus, many new materials are emerging, while old construction techniques are being reconsidered in order to improve their performances. Earth-based construction techniques are viable solutions. Such techniques and materials offer many advantages, but their full-scale use, while respecting actual standards, remains limited.

Considering cob, the objective of present study is to improve this material's thermal properties through phase change materials (PCM) incorporation. Mechanical, hygrometric, and thermal experimental studies were performed on soil-fiber-PCM mixtures. While the incorporation of PCMs showed a clear improvement of cob thermal properties (insulation and inertia), a deterioration of its hygrometric and mechanical properties is observed. Furthermore, energy consumption of a typical house has been estimated by considering cob with different PCM content within its external walls. Finally, an optimum phase change temperature adapted to the Normandy climate has been proposed.

Keywords: cob, heat storage, phase change materials, thermal properties, energy consumption.

1. Introduction

Global warming has already serious consequences on human life. The Intergovernmental Panel on Climate Change (IPCC) predicts an increase in Earth's average atmospheric temperature of 1.5 to 6°C over the next century [1]. This suggested range will depend largely on policies implemented by countries with the highest energy consumption, and then on how they affect the rest of the planet.

Also, IPCC concludes that to stabilize the concentration of greenhouse gases in the Earth's atmosphere at around 457 particles per million (ppm) of CO_2 in 2018, compared to 280 ppm before the industrial era, it would be necessary to reduce greenhouse gas emissions worldwide by half on a global scale by 2050 [2]. In fact, France has already included this objective in its national strategy for sustainable development where residential/tertiary sector is responsible for around 23% of CO_2 emissions in 2018 [3,4].

In term of energy consumption, residential/tertiary sector is responsible for 21 % of global energy consumption in 2018 [4] and 45 % in France in 2019 [4,5]. This sector has significant possibility to save energy through advanced technologies, such as improving the energy efficiency of both technical installations and thermal insulation [6] and per capita energy consumption limitations [7,8].

Substantial energy savings opportunities in heating and cooling can be exploited through better building design, efficient equipment, lighting, and appliances. There are now many examples of net-zero energy buildings [9]. Additional energy savings can be achieved by reducing the embodied energy of building materials [10–12], and more through the increased use of biobased materials [13,14]. It is estimated that the embodied energy, thermal performance, and direct energy use of buildings could reduce emissions by 1.9 $GtCO_2e\ yr^{-1}$ [15]. Even for existing buildings, energy efficiency can be achieved through renovation [16–18] as well as cost savings [6].

To comply with national and international strategies, many thermal and environmental regulations have been imposed. With the implementation of such regulations, new innovative solutions began to emerge in the building wall improvement world. These include the addition of components to cementitious matrices that can improve their thermal behavior, such as the increase of voids in concrete using foam [19] or the inclusion or substitution of lightweight aggregates [20–22]. Foam or lightweight aggregates provide porosity that decreases the thermal conductivity of the material depending on their dosage in the mix.

Another innovative solution aims to limit energy consumption by using bio-sourced materials such as beet pulp starch mixtures [23–25] and earth-based materials [26–34]. The earthen construction techniques well-known since a long time such adobe, cob, light earth, etc., were reconsidered to better understand their thermal, hygroscopic, and mechanical behavior.

The use of earth-based materials in the construction can offer many benefits as particularly the renewability of its main components and low carbon footprint. Soil is one of the natural resources that are often largely available and do not require any specific treatment or transformation. In addition, this resource is sufficiently widespread locally, which reduces transportation emissions and costs. As example, cob, or whatever it is called in the different regions of the world, has been widely used and implemented in various ways. In this regard, cob houses can be found in Canada, USA, Mexico, Mali, etc. [35,36]. In Europe, a comprehensive survey of the earthen building heritage reveals the presence of cob in many countries, namely Austria, Belgium, Czech Republic, Estonia, France, Germany, Hungary, Ireland, Italy, Lithuania, Poland, Portugal, Romania, Slovakia, Slovenia, Spain, Sweden and the United Kingdom [37]. This constructive technique has a particular strong regional presence in northwest France and southwest England.

Raw earth, as well as all earth-based materials, show good hygroscopic behavior for a low economic and environmental cost. In fact, in its raw state, without any additive or firing, the earth proves to be an excellent moisture regulator by its power of absorption and evaporation. It can capture or release moisture from the air according to the ambient humidity, thus promoting a healthy indoor environment [38–44].

This natural way of regulating humidity corresponds to a characteristic missing in conventional building materials such as concrete. That is why interest in earthen constructions has grown these recent years, with many research projects completed and in progress [26,29,31,39,40,45–48]. Most of these investigations focus on improving thermal properties of earth-based materials. For example, one area of particular interest has been the impact of density on the hygrothermal properties of earth-based materials.

Hence, the purpose of investigating earth-based constructions is to find solutions to reduce the energy consumption and the carbon footprint of buildings without degrading the comfort of the occupants. Among the most investigated solutions, heat storage in buildings is a very promising way to rationalize

energy management at the building, district or city level [49]. All materials can release or store heat. Heat storage can occur thermochemically, by the sensible heat or latent heat. In the latter, the energy stored by the material is mass enthalpy of state change. Latent heat storage consists in exploiting the energy involved in a change of body's state. That state change occurs at constant temperature, so it allows to stabilize the temperature for a while at a constant temperature. Such materials are called phase change materials (PCM).

In buildings, phase change materials could be incorporated into walls. As abovementioned, when the outer temperature exceeds the PCM's melting temperature, the material absorbs heat by changing from a solid to a liquid state, delaying heat transfer inside the building. When the temperature falls below the PCM solidification temperature range, the stored heat is released. This leads to more homogeneous inner temperatures, usually close to PCM's melting point. Here, this technology has the added benefit that it shifts the building's heating and cooling load from peak to off-peak periods when considering electricity consumption [50].

There are various methods of incorporating PCMs into building materials:

- Direct incorporation where PCM in liquid or solid state is directly mixed with the construction materials [51–54],
- Immersion where porous building components are immersed in liquid PCM to absorb it by capillary action [55,56],
- Encapsulation where PCM is covered by a micro or macro shell [57–61],
- Shape-stabilized method where PCM is melted and mixed at high temperature with a carrier matrix that retains its shape [62–64],
- Form-stable method in which a carrier matrix retains an optimal percentage of PCM and shows no evidence of leakage during PCM melting. It differs from the shape-stabilized one since the carrier material remains mechanically stable [65,62,66–72].

Incorporating PCM into mortar or concrete has shown promising results in reducing their thermal conductivity and enhancing their thermal mass [37,38] but degrading mechanical performance [73–79]. However, few studies have been focused on PCM addition in earth-based materials [32,80]. Even though many studies have been performed on this field, there is no complete control of these materials' performance.

Present study aims to improve cob's thermal behavior by the use of PCMs. By incorporating PCM directly into the external vertical walls of a cob building, its thermal buffering capacity could be improved, and energy consumption reduced. First, microencapsulated PCMs introduced into earth-fiber mixtures. Samples containing 0 %, 2 %, 5 % and 10 % PCM are formulated. Secondly, soil-fiber mixtures analyzed for their mechanical (compressive strength), thermal (thermal conductivity and specific heat capacity) and hygroscopic (sorption/desorption capacity, water vapor permeability) performances for the different PCM dosages. Then, energy consumption of a typical cob house has been calculated by considering the different PCM content within its external walls.

2. Materials

2.1. Soil

2.1.1. Soil characterization and classification

Cob is an old earth construction technique worldwide known and in all climates. This technique consists of piling up massive, generally load-bearing walls made of soil, water, and plant (or animal) fibers. Cob's composition (soil and fibers) gives it mechanical and hygrothermal properties which contributed to its widespread use through the world in previous centuries.

Suitable soils for cob construction are mainly those presenting a balance between clay, silt, sand and gravel content [81]. In present study, a proportioned soil is obtained by mixing two soils: soil 1 and soil 2. These constitutive soils were characterized to verify their conformity to use guidelines. For this

purpose, a mass of soil 2 is mixed with two masses of soil 1 to obtain the proportioned soil. Soils classification is performed according to the conventional geotechnical characterization respecting applicable standards. The grain size distribution is performed separately for fine particles (laser granulometry with LS 13 320 from Beckman Coulter) and coarse ones (>80 µm) based on XP P94-041 standard [82]. On the other hand, soil plasticity is assessed by Atterberg's limits following NF EN ISO 17892-12 standard [83]. Thus, Soil liquidity limit (LL), plasticity limit (PL) and plasticity index (PI) are determined. Clay activity is given by methylene blue value (MBV) following NF P94-068 standard [84]. Using these characteristics, soil classification based on Unified Soil Classification System (USCS) becomes possible.

Soils nature and parameters are presented in Table 1 and shown in Figure 1.

Table 1:Atterberg limits, methylene blue values and soil classification.

Soil	LL [%]	PL [%]	PI [%]	MBV [g/100g]	USCS [85]
Soil 1	27.6	24	3.6	1.61	Low plasticity silt (ML)
Soil 2	23.7	21	2.7	0.47	Silty sand with gravel (SM)

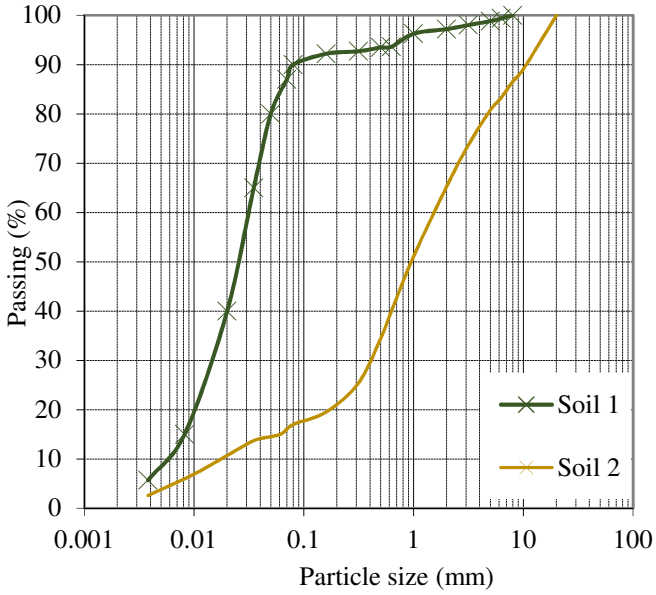

Particle size	Soil 1 [%]	Soil 2 [%]
< 2 µm	4	1
2-20 µm	36	10
20-50 µm	40	3
50-200 µm	12	8
0,2-2 mm	5	43
>2 mm	3	35

Figure 1: Soils particle size distribution.

2.1.2. Chemical and mineral composition

The chemical and mineral compositions of soil are performed at CRISMAT laboratory (ENSICAEN-University of Caen Normandie, France) by X-Ray Fluorescence (XRF) and X-Ray Diffraction XRD techniques. The Inel Equinox 3500 spectrometer is used to collect the X-ray fluorescence spectra. Data are collected with an integration time of 400 s. Then, X-ray powder diffraction diagram is collected using a pure copper K radiation (= 1.54059) selected by an incident beam Ge (111) monochromator on a D8 Advance Vario 1 Bruker instrument. The X-ray diffraction pattern of soil is collected for 1sec each 0.01° step (16 h/scan) from 10° to 80°.

XRF technique revealed that the soil 1 used in this study contains mainly silicon, aluminum, iron and sodium for the major cations, see Table 2.

Table 2: chemical composition of structural soil in weight obtained by XRF measures.

Element	%
Silicon dioxide (SiO_2)	65.89
Aluminum oxide (Al_2O_3)	14.23
Ferric oxide (Fe_2O_3)	6.65
Magnesium oxide (MgO)	4.08
Potassium oxide (K_2O)	2.17
Titanium dioxide (TiO_2)	2.08
Calcium oxide (CaO)	1.27
Sodium oxide (Na_2O)	1.11
Manganese oxide (MnO)	0.16
Phosphorus Pentoxide (P_2O_5)	0.14
Sulfur trioxide (SO_3)	<0.1
Loss on ignition	2.26

XRD analysis is performed to achieve the mineralogical composition of soil 1. The online Full Profile Search Match fitting process (FPSM) is used to do a preliminary quick phase analysis [86]. The FPSM tests all probable crystal structures from the COD Database (limited to the XRF-detected elements) using a Rietveld fitting process, resulting in an ordered list of candidates for further quantification, see Figure 2. The soil's XRD pattern is then Rietveld-fitted, with the preceding phase identification taken into account [87]. The general R-factors, indicating the overall goodness of fit between the model and experimental data, are: Rwp = 5.3% and Rb = 3.9%, giving fit goodness of 1.8. The microstrain values are also fitted during this step and remain low for all the phases.

According to quantitative phase analysis using Rietveld refinement, the XRD diagram is indexed by the following major phases: quartz (54.8 %), muscovite (26.2 %), montmorillonite (6.9 %) and albite (4.2 %), with minor occurrences of Kaolinite, goethite, rutile, illite and huntite. This allows to affirm the silty nature of soil 1.

Soil 2 (silty sand with gravel) is a French natural sand made by Société des Sablières du Cotentin (SABCO, Lieusaint). It is composed by natural silica sand (Quartz). The grains are washed and of rounded shape.

Thus, the major phases in both soils are primary minerals. Quartz is the first mineral in the soils. Mica, feldspars, iron oxyhydroxides, and limonite are other minerals commonly found, but in lower concentrations [88].

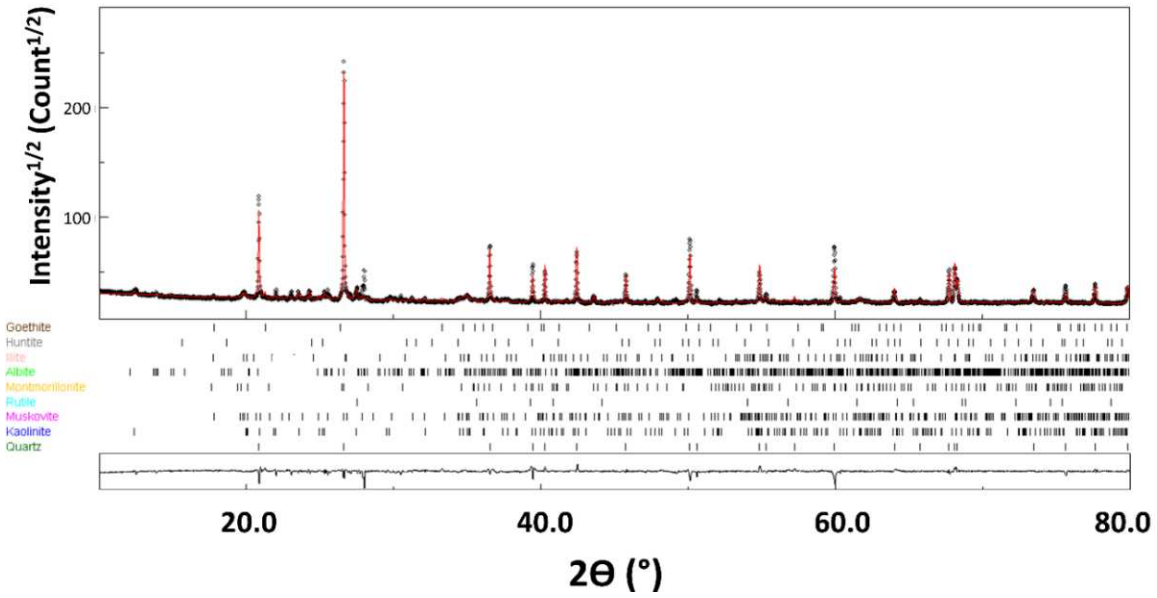

Figure 2: XRD pattern of structural soil. On top of the observed profile, the computed pattern (red line) is superimposed (black dots). At the bottom is the difference curve (Iobs – Icalc).

Table 3: Refined values of lattice parameters, unit cell volume, average diameter and microstrain <ε2>1/2 used. One standard deviation is indicated in parenthesis on the last digit.

Phases	**COD reference**	**V (%)**	**Lattice type + Space group**	**Lattice parameters (Å)**	**⟨D⟩ (nm)**	**$\langle\varepsilon^2\rangle^{1/2}$**
Quartz **SiO_2**	1526860	54.8 (5)	Trigonal $P3_221$	a=4,914 (2) c=5,405 (2)	492 (10)	$5.\ 10^{-4}$
Muscovite **$KAl_2(AlSi_3O_{10})(F,OH)_2$**	1100011	26.2 (5)	Monoclinic C2/c:b1	a=5,194 (1) b=9,005 (2) c=19,995(1) β=95.782 (1)	35 (5)	$6.\ 10^{-3}$
Montmorillonite **$(Na,Ca)_{0.3}$** **$(Al,Mg)_2Si_4O_{10}(OH)_2$**	1100106	6.9 (2)	Monoclinic C2/c:b1	a=5,386 (2) b=9,039 (2) c=10,196(2) β=100.457 (2)	111 (6)	$6.\ 10^{-4}$
Albite **$NaAlSiO_3$**	1556999	4.2 (2)	Triclinic P1	a=8,166 (1) b=12,845 (1) c=7,188 (1) α=94.240 (1) β=116.590 (1) γ=87.715	43 (5)	$6.\ 10^{-3}$
Kaolinite **$Al_2Si_2O_5(OH)_4$**	1011045	2.1 (3)	Monoclinic Cc:b1	a=5,185 (1) b=8,885 (1) c=14,526 (1) β=100.662 (1)	78 (5)	$6.\ 10^{-4}$
Goethite **α-FeO(OH)**	2211652	2.0 (3)	Orthorhombic Pbnm:cab	a=4,579 (1) b=9,945 (1) c=2,998 (1)	21 (1)	$6.\ 10^{-4}$
Rutile **TiO_2**	1532819	1.6 (3)	Tetragonal P42/mnm	a=4.582 (1) c=3.014 (2)	92 (5)	$8.\ 10^{-4}$
Illite **$(K,H_3O)(Al,Mg,Fe)_2(Si,Al)_4O_{10}[(OH)_2,(H_2O)]$**	2300190	1.1 (2)	Monoclinic C2/m:b1	a=5,197 (1) b=8,961 (1) c=10,159(1) β=100.970 (1)	100 (5)	$6.\ 10^{-4}$

Huntite $Mg_3Ca(CO_3)_4$	1000046	1.1 (2)	Trigonal R32:H	a=9,502 (2) c=7,821 (2)	123 (5)	$8.\ 10^{-4}$

2.2. Fiber

To prepare cob material, flax straw was selected and incorporated into the soil with a proportion of 2.5 % of dry soil mass. Flax straw is porous (Figure 3) with high tensile strength which improves cob mechanical behavior. The flax straw is cut to a length of 7±1 cm. It should be noted that flax straw is poor in fibers.

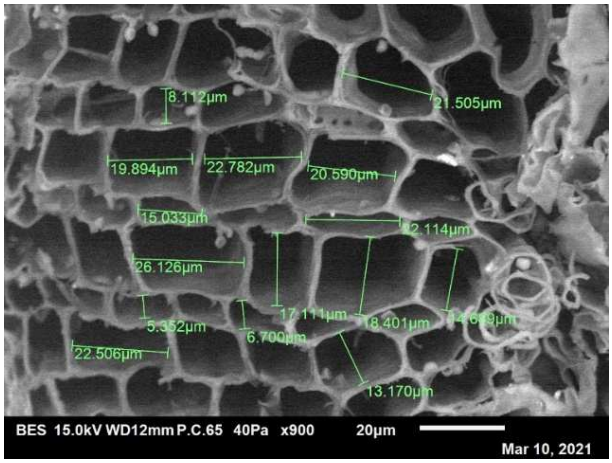

Figure 3: MEB image representative of the used porous flax straw.

2.3. Phase Change Materials (PCMs)

For the sake of energy saving, PCMs incorporated in building walls must present an appropriate phase change temperature. This depends on the building environment. When considering the average temperature in France, which varies between 0 °C and 30 °C [89], and human thermal comfort, phase change temperature should be within the 16-25 °C range [90]. If melting/solidification temperature is an important criterion to take into account when selecting a PCM, it is also important to consider other parameters *i.e. latent heat of phase change, chemical properties, etc.* On an other hand, microencapsulated PCMs are preferred to bulk ones to avoid their leakage as well as providing a higher heat transfer surface per unit volume [91].

In accordance with the above-mentioned criteria and commercially available PCMs, Micronal DS 5038 X has been selected. This PCM has favorable thermal properties. Its melting temperature (24 °C) is suitable for the French climate and human thermal comfort application. Micronal DS 5038 X is made from a paraffinic core and acrylic shell. The data provided by the supplier [92] have been checked and confirmed in laboratory. On Figure 4, melting and solidification of the PCM can be seen around 21 °C and 23 °C, respectively. Peaks around -7 °C can also be seen. These peaks are supposed due to transformations happening in the polymeric shell of the PCM [93]. These are not taken into account in the numerical simulation. Micronal DS 5038 X physical properties are presented in Table 4 and Figure 4.

Table 4: Micronal DS 5038 X physical properties

Micronal DS 5038 X	**Particle size [µm]**	**Bulk density [kg/m³]**	**Temperature [°C]**		**Latent heat [J/g]**	
			Melting	**Crystallization**	**Melting**	**Crystallization**
	50-300	300-400	21	23	97	98

Note: Differential scanning calorimeter DSC at 1 K/min

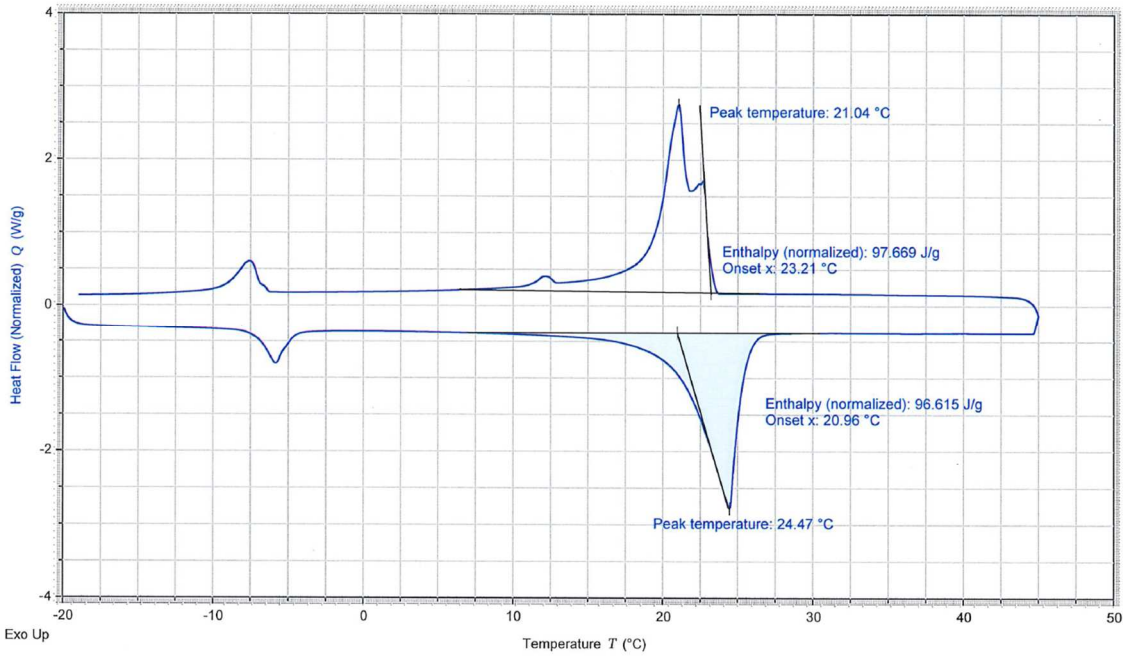

Figure 4: Micronal 5038 X melting/crystallization DSC curves [92].

2.4. Preparation of cob samples

Cob is basically made of soil, fiber, and water. In present study, PCMs have been incorporated with different quantities. The various weight ratios of cob-PCM mixtures are as follow: water/soil ratio is equal to 0.3, fiber/soil ratio is equal to 0.025 and PCM/(soil+fiber) ratio varies from 2 % to 10 %, see Table 5. Before mixing and manufacturing, raw materials were previously dried during 2 weeks in an oven at 40 °C, then covered and placed at room temperature *i.e. 20 °C*. Raw materials densities and cob formulations are presented in Table 5 and Table 6, respectively.

Table 5: Raw materials densities.

Raw materials	**Soil**	**Fiber**	**Micronal DS 5038 X**
Absolute density [kg/m^3]	2600	1250	1100

Table 6: Cob formulations (kg/m^3).

Formulation [kg/m^3]	**Cob0**	**Cob2**	**Cob5**	**Cob10**
Soil	1500	1475	1450	1390
Fiber	37.5	36.9	36.3	34.8
Water	375	368	362	347
Micronal DS 5038 X	0	30.2	74.3	142.5
f/s [wt.%]*	2.5	2.5	2.5	2.5
w/s [wt.%]*	30	30	30	30
PCM/(s+f) [wt.%]*	0	2	5	10

* Soil, fiber, water, and phase change material are indexed with s, f, w and PCM, respectively.

First, soils are sieved down to 20 mm. Fractions larger than 20 mm are eliminated. A common preparation procedure is used for all test samples. After weighing, soils and PCMs are firstly hand-mixed in a dry state to ensure a homogeneous distribution. Then the required water quantity is added

and followed by flax straw while continuing the mixing. Mixture is carried out in a concrete mixer (PROVITEQ 65 L) for 2 minutes. Once mixing is complete, the cob-PCM mixtures are bagged and stored at room temperature, *i.e. 20 °C*. One day later, this mixture is compacted manually with a wooden plate in pre-oiled molds. There are two types of molds: prismatic molds enabling samples for thermal testing (30 x 30 x 4 cm^3) and cylindrical molds enabling samples for compressive strength testing (diameter Ø11 cm x height 22 cm). The next day, samples are put into an oven at 40°C. In the case of cylindrical samples, the molds are completely removed after two days. For the prismatic samples, molds are partially removed: only one side every 2 days. The complete drying process takes place over approximately 3 weeks. A sample is considered dry when its mass does not differ more than 0.1 % between two daily weight measurements. Before testing, the pre-dried samples are placed in a room at 20°C and 50% relative humidity for about 7 days.

3. Experimental methods

3.1. Physical properties

Porosity and bulk density are important physical parameters to consider when studying building materials. Knowing their values will ease interpretation of a possible evolution of cob-PCM properties. Since water cannot be used with earth-based materials, these physical properties are measured by immersing small samples in a non-wetting oil (dearomatized oil). Experiments are carried out according to NF ISO 5017 [7].

First, the samples are dried to remove water from the materials pores. Afterward, the cob-PCM samples are saturated by oil under vacuum. Then, these were weighed while submerged in oil and again weighed in air. Samples are dried until a constant mass is obtained*, i.e. when two successive daily weight measurements do not differ by more than 0.1 %.* This is dry mass. This method makes it possible to obtain, by means of a difference in mass between saturated and dry states, both void volumes initially filled with oil and sample bulk density. Thus, accessible porosity p_0 is given by equation (1) and bulk density ρ_{sp} by equation (2).

$$p_0 = \frac{M_a - M_s}{M_a - M_o} \tag{1}$$

$$\rho_{sp} = \frac{M_s}{M_a - M_o} \times \rho_o \tag{2}$$

Where, M_s is mass of dry specimen, M_a, the mass of saturated specimen weighed in air, M_o, the is mass of saturated specimen weighed in oil, ρ_{sp}, the specimen bulk density and ρ_o, is the oil bulk density.

3.2. Mechanical behavior

The cob mechanical strength is expected to be adequate to build a few-story buildings. The main mechanical parameter of cob is its compressive strength. To analyze how PCM incorporation affects its mechanical performance, unconfined compressive strength (UCS) tests have been performed. This is conducted according to EN 1015-11 standard [94]. Samples diameter is 11 cm and height is 22 cm as shown on Figure 5.

Tests were performed under a controlled force. Stress-strain curve is deduced from the displacement and force measurements from the sensors integrated in the press. The slenderness, ratio between height and diameter, is equal to 2. Three samples each formulation prepared and tested. UCS was obtained with

an INSTRON SCHENCK press of 100 kN capacity. The compressive strength throughout the test is calculated according to equation (3):

$$R_{c,i} = \frac{F_{c,i}}{A} \tag{3}$$

Where, $R_{c,i}$ is the unconfined compressive strength at a strain value i [MPa], $F_{c,i}$, the compressive load for strain value i [N] and A, the cross-section area of the sample [mm^2].

Figure 5: Cob sample to be tested under the INSTRON SCHENK press.

3.3. Hygroscopic behavior

3.3.1. Water vapor permeability

The water vapor permeability of a material represents its ability to allow vapor to pass through when exposed to a difference of water vapor pressure between its both sides. In this study, water vapor permeability of the prepared samples is measured according to the standard ISO 12572 [95] using the dry cup method. All samples were preconditioned at 23°C and 50% relative humidity (RH). This method gives information about material behavior when moisture transfer is dominated by vapor diffusion. This dry method requires to create a moisture gradient from inside the cup (≈ 0% RH) to outside (≈ 50% RH) across the specimen.

Specimens are sealed onto the test cup containing a desiccant (in this case silica gel). The whole assembly (cup, desiccant and sample) is then placed in a temperature and humidity-controlled climatic chamber at 23 °C and 50% RH. Due to partial vapor pressure difference between the cup and the chamber, water vapor diffuses through the cob. The assembly is periodically weighed to determine steady-state water vapor transmission rate.

In steady state, water vapor flux (G) through the sample is given by the regression line slope of cup-sample assembly mass versus time. This result is obtained after removing the initial nonlinear test phase. To achieve this, five aligned points must be obtained that differ by no more than 5% from the line.

This water vapor flux is used to calculate the sample water vapor resistance (Z) from the water vapor permeance (W) using equation (4) by considering the difference in water vapor partial pressure between sample sides (ΔP_v).

$$Z = \frac{1}{W} = \frac{A \times \Delta P_v}{G} \quad (4)$$

It is possible to determine sample water vapor permeability (δ) by using equation (5) in which e is the sample thickness.

$$\delta = W \times e \quad (5)$$

Eventually, the sample water vapor resistance factor (μ) is obtained according to equation (6). δ_a is the air vapor permeability at atmospheric pressure which is equal to 2×10^{-10} kg.m^{-1}.s^{-1}.Pa^{-1}.

$$\mu = \frac{\delta_a}{\delta} \quad (6)$$

3.3.2. Moisture sorption isotherm

The second hygrometric parameter investigated is the sorption/desorption. It describes a material ability to absorb and release moisture from the environment. The technique of dynamic vapor sorption (DVS) is used according to ISO 12571 standard [96]. A ProUmid SPSx-1μ sorption/desorption analyzer is used. The device has a precision balance (±1 μg) and tight temperature and humidity control which allows accurate measurements of sample mass and sorption kinetics. The sample is exposed to different successive steps of increasing and decreasing ambient relative humidity to obtain adsorption/desorption isotherm curves. Results are presented in terms of sample water content versus relative humidity.

Samples of approximately 30x30x30 mm^3 are dried until the mass stabilizes, *i.e. weight change less than 0.1 %.* Thereafter, the samples are exposed to an atmosphere with a relative humidity varying from 10 % to 90 % in 5 steps, keeping experiment temperature at 23 °C. In accordance with the standard, a sample is considered at equilibrium when the mass variation is less than 0.1 % for three consecutive mass measurements performed at least 24 hours interval.

Determination of moisture sorption isotherms and water vapor permeability allows evaluation of PCMs impact on cob hygroscopic behavior.

3.4. Thermal behavior

3.4.1. Thermal conductivity

The cob thermal behavior is being investigated. Thermal conductivity (λ) is a physical parameter that characterizes a substance ability to conduct heat. The appropriate methodology to determine this property depends on nature, shape and sample size being studied. In this study, thermal conductivity measurements are performed with an HFM 436 Lambda calorimeter. This method consists in generating a temperature gradient between two plates through the material under study having a surface (A) and thickness (e). Heat flow into and out of the material is measured using heat flow sensors placed in each plate. When the equilibrium state is reached and the heat flow ($\dot{Q}$) is constant, the material thermal conductivity is calculated using Fourier's law [97] through equation (7).

$$\lambda = \frac{\dot{Q}}{A}\frac{e}{\Delta T} \quad (7)$$

Thermal measurements were performed on 30 x 30 x 4 cm^3 prismatic samples at different average temperatures *i.e. 14, 24 and 34 °C.* These temperatures were chosen based on the phase change material and its melting temperature: one measurement in phase change range (24 °C) and two other measurements out of phase change, in solid state (14 °C) and liquid state (34 °C). The temperature difference between both sides is set to a value of 10 °C for each measurement.

3.4.2.Specific heat capacity

Specific heat capacity (Cp) is a key parameter indicating the ability of a material to store heat. Differential Scanning Calorimetry (DSC) is generally used to determine this parameter according to the standard ISO 11357-4 [98]. The test consists in a scan of temperature and following the heat flow into or out of the studied material compared to a reference. In present work, samples specific heat capacity is analyzed between 0 °C and 40 °C. Heating rate is fixed at 1 °C.min^{-1}.

DSC measurements are performed on raw materials (few milligrams) and, as this study deals with multicomponent mixtures, the mixing law has been applied. Equation (8) is used to determine the mixtures specific heat capacity at each temperature [26].

$$Cp = F_s . Cp_s + F_f . Cp_f + F_{PCM} . Cp_{PCM} \quad (8)$$

In equation (8), component specific heat capacity and mass fraction are presented as Cp and F, respectively. Soil, fiber, and phase change material are indexed with s, f and PCM, respectively.

4. Numerical simulation of energy consumption

In order to investigate an eventual energy saving allowed by cob incorporating PCMs, numerical simulations are undertaken on a typical individual house. In such simulations, special attention should be paid to several factors concerning the PCM in particular and the building envelope in general: PCM content, melting/solidification temperature, latent heat of phase change, envelope design, etc.

In present study, the annual energy consumption is simulated by considering the different PCM content in the external cob walls of single-family house.

After exploring the different numerical tools that can be suitable for present work calculations, EnergyPlus was found to be the more appropriate. For practical purposes, calculations are performed under the DesignBuilder interface. These simulations are based on the cob-PCM properties determined experimentally and in part on those given by the PCM manufacturer.

The simulated housing is supposed to be located in Caen (France). In this city, weather is partly cloudy throughout the year. Summers are comfortable while winters are long, cold, and windy. During the year, temperatures generally vary between 2 °C and 20 °C and are exceptionally below -3 °C or above 28 °C.

A one-story house with vertical external walls made of cob incorporating PCM is considered. Its other parts remain unchanged and will not contribute to energy consumption changes. The house living space is 95.11 m^2 (Figure 6) to be heated and cooled throughout the year according to the following scenario.

A family of 4 persons occupies the house at a rate of 0.042 person/m^2 throughout year from 4pm to 9am and all weekends. The whole house requires heating and/or cooling when the occupants are present and awake, *i.e., from 7 to 9am and from 4 to 11pm*. The target temperatures for heating and cooling are respectively 19 and 25 °C. These temperatures are in the human thermal comfort zone. Outside these periods, cold and hot temperature can reach 16 and 28 °C, respectively. Timing and temperature setpoint are presented in Figure 7.

To numerically represent PCM embedded in the cob, the composite is considered as 50 cm thick. Its properties are those determined experimentally: density, thermal conductivity, specific heat capacity and water vapor permeability. The input value of the composite latent heat is equal to the PCM latent heat multiplied by its proportion within the composite. The suitable PCM modeling option in EnergyPlus is the hysteresis method. This method allows the PCM to follow different temperature/enthalpy curves during melting/solidification processes and therefore, to approach the real behavior of building envelopes integrating phase change materials.

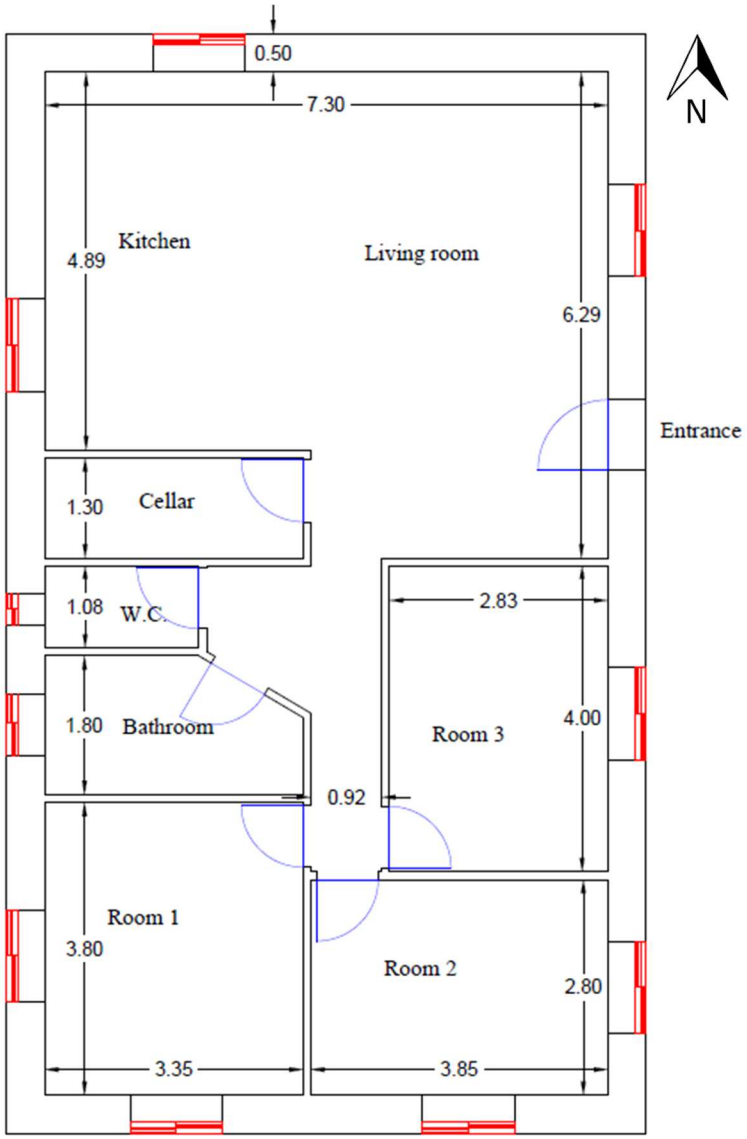

Figure 6:2D plan of the studied house.

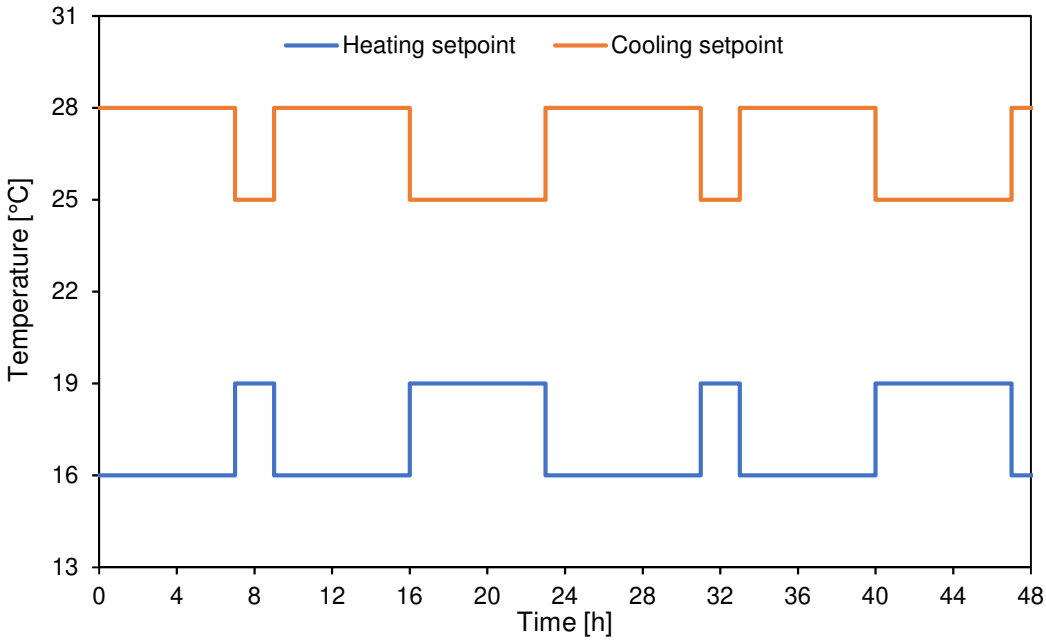

Figure 7: Adopted weekly heating/cooling scenario (except weekend).

5. Results and discussion

5.1. Physical properties and mechanical behavior

From Figure 8, it can be seen that both density and open porosity decrease with PCM incorporation within cob. In fact, the Micronal DS 5038 X present a density of 300-400 kg.m^{-3}. Adding a lighter material to cob leads to a decrease in its primary density (≈ 1500 kg.m^{-3}). Elsewhere, the decrease in porosity can be explained by the fact that PCM particles (50-30 µm) feed into the pores within the mixture.

Incorporation of Micronal DS 5038 X will result in a decrease in cob mechanical strength. Indeed, the cob's Unconfined Compressive Strength (UCS) decreases, and the material becomes more ductile, see Figure 9. This might be due to the fact that PCM addition will reduce the cohesion between soil particles and flax straw.

Regarding literature, several compressive strength analyses were conducted on cob mixes. Reported results reveal a compressive strength equal to 0.12 MPa [99], 0.6 MPa [100], 1.2 MPa [101] and can reach 1.6 MPa [102]. However, in this work, the lowest compressive strength measured (cob10) is equal to 1.5 MPa, see Table 7. This strength is considered sufficient to build a two-story or even a three-story dwellings [99,100].

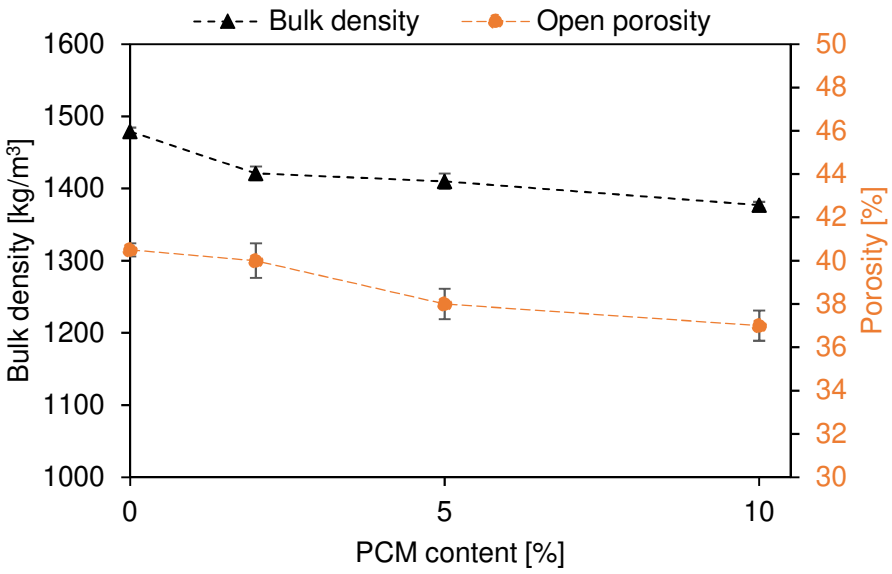

Figure 8: Cob's density and open porosity variation versus PCM content.

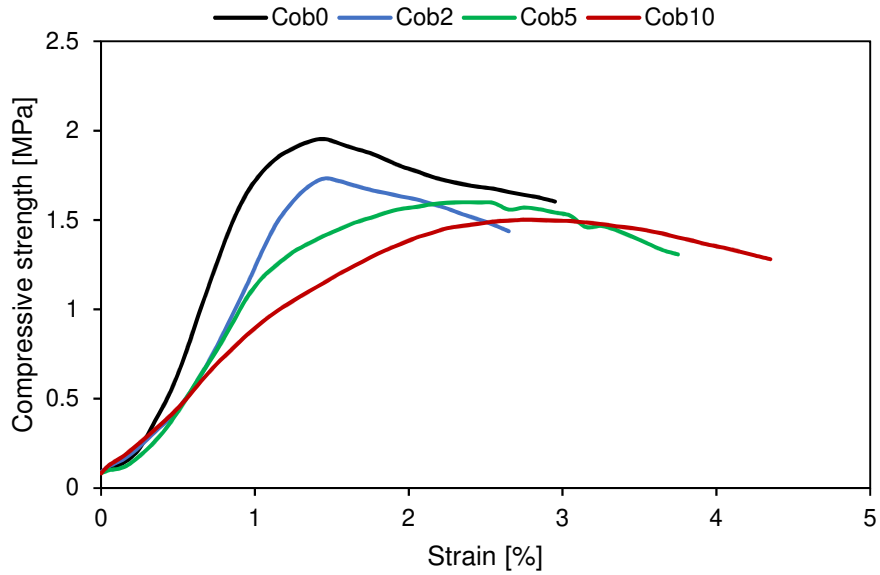

Figure 9: Stress-strain relationship of cob as function of PCM content.

Table 7: Maximum values of Cob's compressive strength versus PCM content

Samples	Cob0	Cob2	Cob5	Cob10
Compressive strength [MPa]	1.95	1.73	1.60	1.50
Strain [%]	1.45	1.45	2.35	2.75

5.2. Hygroscopic behavior

5.2.1. Water vapor permeability

From Figure 10, it can be seen that the value of the water vapor resistance factor (μ) of the cob0 is relatively close to the one reported by Phung ($7 < \mu < 10$) [29] or ($4 < \mu < 10$) [103] and not far from $\mu = 8$ [104] and $\mu = 13.3$ [105]. Also, it can be observed that water vapor permeability decreases

proportionally with PCM content. The drop in water vapor permeability is equal to 11 %, 16 % and 33 % for cob2 cob5 and cob10, respectively. Certainly, an increase can be observed on the curve representing evolution of water vapor resistance factor. Clearly, this means that cob loses its ability to let moisture pass through. This decrease in permeability can be correlated to the drop in porosity. Moreover, since Micronal DS 5038 X present a hydrophobic shell, this characteristic might also affect cob's hygroscopic behavior, including its water vapor permeability.

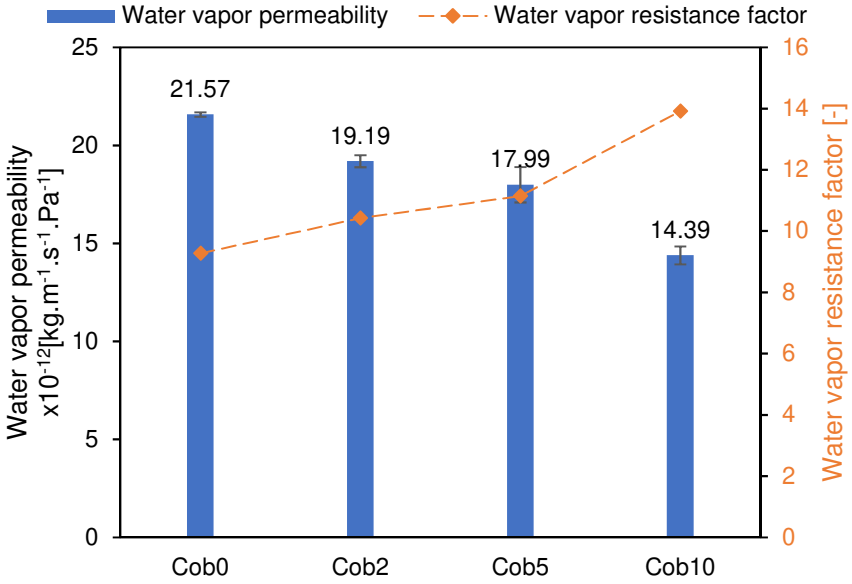

Figure 10: Water vapor permeability and resistance factor measured for cob-PCM mixtures compared to cement mortar [106].

5.2.2. Moisture sorption isotherm

On Figure 11 moisture sorption isotherms of the different studied mixtures are shown. The curves represent evolution of moisture content in the cob-PCM mixtures versus ambient air relative humidity at a temperature of 23 °C. It can be seen that addition of PCM into cob implies a decrease in the amount of its absorbed moisture. This is supposed due to the hydrophobic nature of the Micronal DS 5038 X. As illustration, at a relative humidity of 90%, moisture absorbed into cob reaches 2.5% of the sample mass. The drop due to PCM content is equal to 3 %, 10 % and 17 % for cob2 cob5 and cob10, respectively at RH equal to 90 %.

Otherwise, when looking sorption and desorption curves, a hysteresis can be observed. This latter decreases slightly with PCM addition in accordance with porosity decrease. It is mean that cob and cob-PCM mixtures can release the totality of the absorbed water vapor and retrieve their initial state.

Finally, whether sorption or water vapor permeability, adding PCM slightly degrades the hygroscopic character of cob, but these properties remain comparable to those of other earthen-based materials *i.e. the moisture content absorbed by cob at 90% relative humidity varies between 2.8 % and 3.7 %* [29].

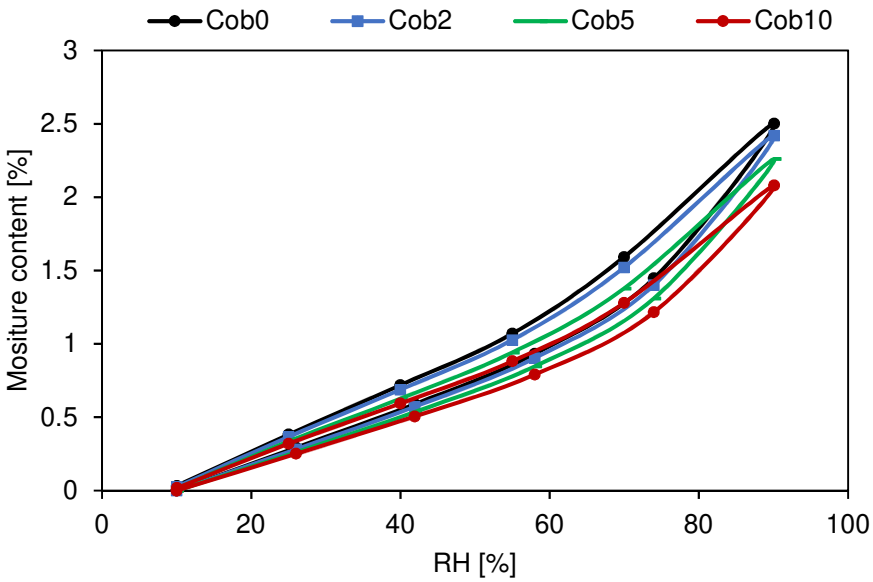

Figure 11: Moisture sorption isotherm of cob with different PCM content

5.3. Thermal behavior

5.3.1. Thermal conductivity

As it can be seen on Figure 12, thermal conductivity (λ) of cob-PCM mixtures is measured at three different temperatures (14 °C, 24 °C, and 34 °C) *i.e. before, during, and after phase change*. The microencapsulated PCM is in a solid form at 14 °C, and in a liquid form at 34 °C. Results presented in Figure 12 show a thermal conductivity ranging between 0.64 and 0.76 W/(m.K) close as well as the one reported between 0.4 and 0.7 W/(m.K) [105]. Therefore, these results indicate that cob thermal conductivity decreases with PCM incorporation rate. This is supposed due to the low thermal conductivity of the PCM itself. Micronal DS 5038 X present a thermal conductivity of about 0.08 W/(m.K). This value was given by the supplier and verified in laboratory.

Moreover, this decrease in thermal conductivity is relative to the drop in the density. Previous studies [26] revealed the correlation between thermal conductivity and density of a material. λ increases with increasing density and conversely.

Thermal conductivity stabilizes at 5 and 10 % PCM content with an approximate 15 % reduction. This provides an indication for an optimal amount of PCM to be added. Optimum PCM content must be defined according to different properties and nature of materials. As an example, according to studies carried out on this issue, 20 % PCM has been indicated as optimum for a standard cement mortar [74] and 10 % for light earth when comparing thermal conductivity [32]. This value is strictly based on thermal conductivity. However, to achieve an ideal optimum, different behaviors need to be studied. Numerical simulation could be useful for this purpose. Lastly, it can be stated that Micronal DS 5038 X improves cob insulating properties as a function of its incorporation rate and temperature.

Otherwise, it can be seen that temperature has almost no effect on cob's thermal conductivity. In fact, at the three temperatures (14 °C, 24 °C, and 34 °C) at which thermal conductivity is investigated, no significant evolution has been observed. Despite the phase change expected at 24 °C leading to more disorder in the PCM, no noticeable variation has been registered. This can be supposed due to the fact that at this temperature, the PCM is already melt.

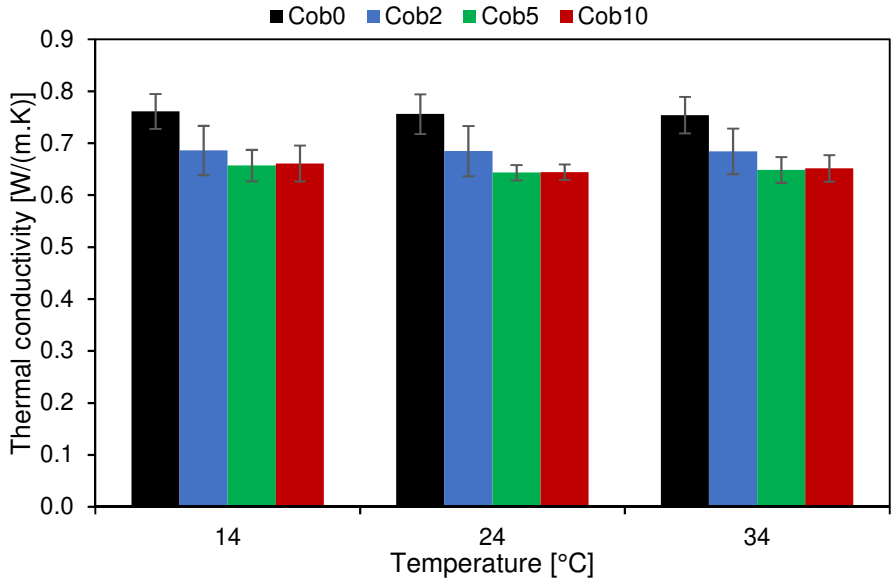

Figure 12: Thermal conductivity of cob mixtures as function of temperature and PCM content.

5.3.2.Specific heat capacity

The evolution of raw materials and mixtures specific heat capacity as function of temperature is presented in Figure 13 and Figure 14, respectively. As expected for such materials, the Cp value increases with temperature. Regarding the PCM effect, results analysis can be divided into 2 parts, out and within phase change zone. Out of this zone, Micronal 5038 X addition improves cob Cp value. The increase is linear with PCM content. Outside the phase change zone, specific heat capacity is approximately 3 %, 7 %, and 14 % higher than the one of the control sample for 2 %, 5 %, and 10 % PCM content, respectively. Peaks in Cp values are seen within the phase change zone. Peak values of cob2, cob5, and cob10 are approximately 55 %, 132 %, and 252 % higher than the Cp of cob0 at the same temperature. For example, cob specific heat capacity increases from 1164 $J.kg^{-1}.K^{-1}$ for cob0 to 3862 $J.kg^{-1}.K^{-1}$ with 10 % PCM added (cob10) at ≈ 24 °C. This improvement is due not only to material sensible heat, but also to the latent heat released/absorbed during the material phase change.

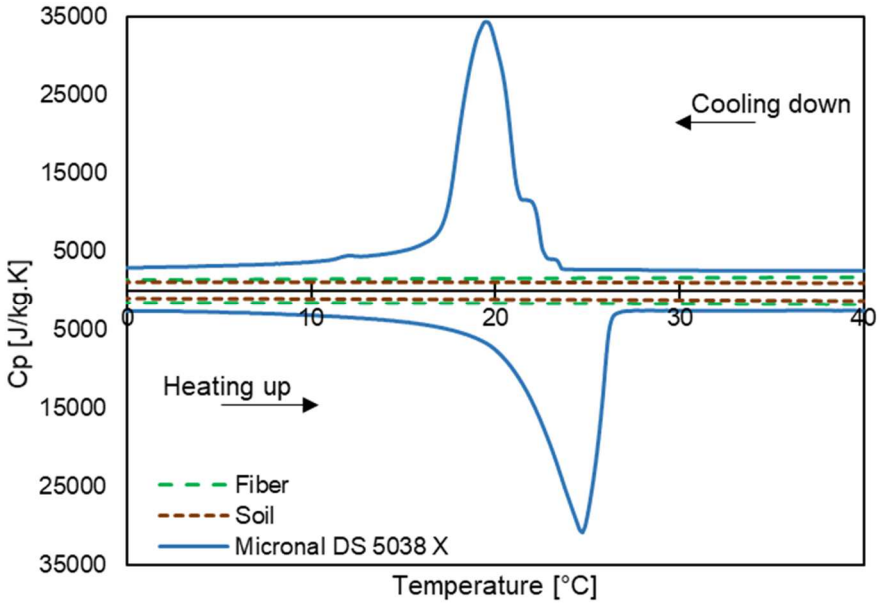

Figure 13: Evolution of the raw materials specific heat capacity as function of temperature.

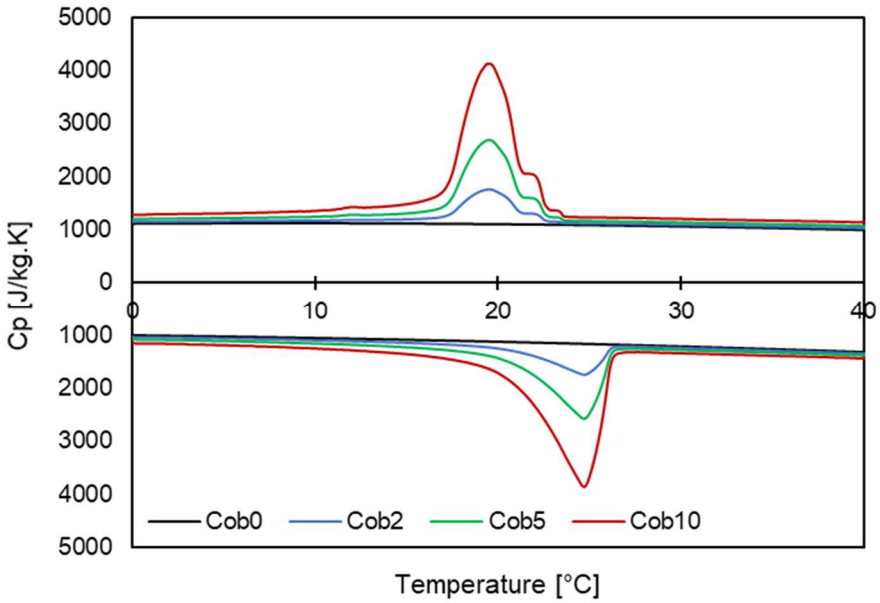

Figure 14: Evolution of the cob's specific heat capacity as function of temperature and PCM content.

5.4. Results of the numerical simulation

The energy consumption simulation is performed over one year. Results show a decrease in energy consumption for heating and cooling. Consumptions due to other uses i.*e. lighting load, sanitary water load etc.* were kept unchanged when simulating the different formulations.

Results reported in Figure 15 show a decrease in energy consumption due to the drop in heating and cooling needs. Thus, energy savings rise with the increase of PCM content. In Caen, the need for heating is higher than the need for cooling. Both requirement changes from 4625 kWh/year to 4316 kWh/year for 2 %, to 4100 kWh/year for 5 % and 4036 kWh/year for 10 % of PCM content, see Figure 15. This means that heating and cooling needs decrease by 6.7, 11.3 and 12.7 % with 2, 5 and 10% PCM content, respectively.

To know if results reported on Figure 15 are the maximum gains that can be reached in Caen, an investigation of the energy savings as function of phase change temperature has been performed.

Therefore, the same phase change material is assumed, with the same properties except phase change temperature. The formulation cob10 has been selected and phase change temperatures ranging from 14 to 26 °C with a step of 2 °C have been considered. The results of the calculations are presented on Figure 16. From this latter, it can be found that a phase change temperature between 18 and 20 °C allows more energy savings. Within this temperature range, energy savings when considering heating/cooling needs exceed 25 %. Consequently, it can be stated that a phase change temperature of 18 °C is more adequate than 24 °C for the Caen's climate.

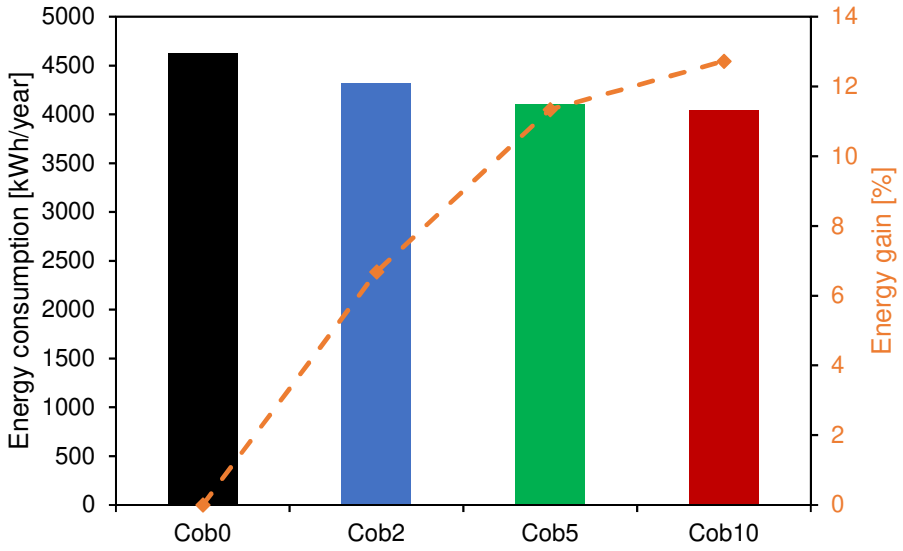

Figure 15: Annual energy consumption due to heating/cooling and energy gain rate when considering cob house with different PCM content in its external walls.

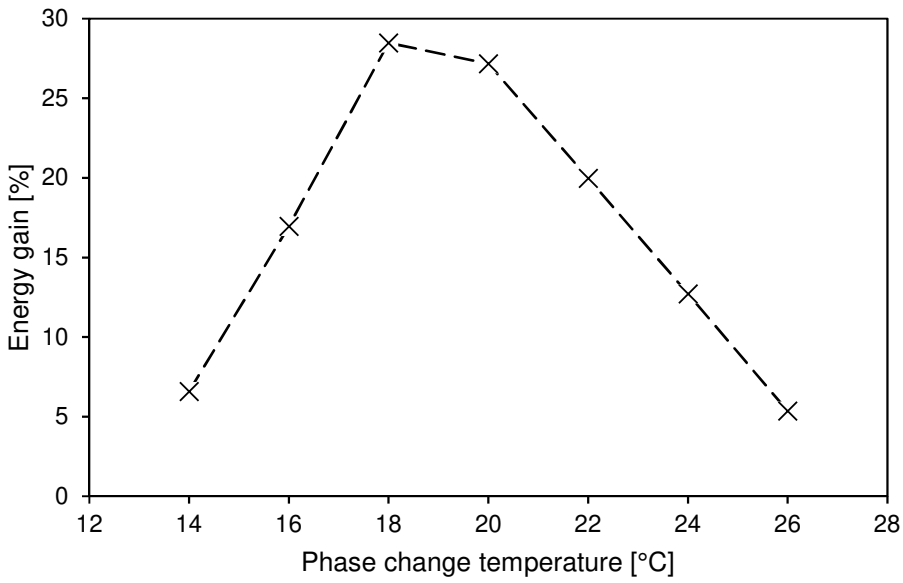

Figure 16: Impact of phase change temperature on energy savings in a cob house containing 10% PCM in its external walls when considering the Caen's climate.

6. Conclusion

Present work aimed to evaluate the effect of PCM addition on cob's thermal, hygroscopic, and mechanical properties. Thus, samples of cob with various PCM content were formulated and investigated. Thermal conductivity, specific heat capacity, moisture sorption isotherms, water vapor permeability and compressive strength were experimentally studied. Then, the experimental work was completed with a numerical simulation. These calculations aimed to evaluate energy savings resulting from PCM incorporation into cob and also to determine the optimal phase change temperature for the Caen's climate. To do so, a typical one-storey house has been considered.

Experimental studies revealed that incorporation of PCMs into cob improves its insulation ability, heat storage capacity while degrading its mechanical and hygroscopic properties. Despite this, cob incorporating PCMs remain sufficiently resistant to support up two levels buildings and enough hygroscopic when compared to other conventional and earth-based materials. Thus, cob with 10% of PCM content loses almost 20% of its compressive strength when compared to the one without PCM. This loss is associated with a ductile behavior of cob.

Elsewhere, cob is considered as a hygroscopic material (permeable to water vapor and capable to absorb and release moisture from the environment). PCM addition degrades cob's hygroscopic behavior. Indeed, cob sorption behavior and water vapor permeability are inversely proportional to PCM content. The water vapor permeability drops by 11 %, 16 % and 33 %, and the sorption behavior at RH equal to 90 % decreases by 3 %, 10 % and 17 % for cob2, cob5, and cob10, respectively. This drop is supposed due to PCM's hydrophobic nature and decrease in the mixture open porosity.

The experimental studies showed that addition of Micronal DS 5038 X into cob decreases its thermal conductivity of approximately 9 % for cob2 and 15 % for cob5 and cob10. Thus, the mixture insulating ability is increased consequently. This decrease is supposed due to the PCM's thermal conductivity much lower than the cob's one. When considering temperature effect, at 14 °C, 24 °C, and 34 °C, thermal conductivity did not show any significant change. Moreover, PCM incorporation has shown an interesting effect on cob's specific heat capacity. Indeed, it is observed that Cp increases linearly with PCM content outside the phase change zone. When PCM content is 2 %, 5 % and 10 %, Cp value is respectively 3 %, 7 % and 14 % higher than that of the reference sample when heating up or cooling down. These improvements are almost identical before and after the phase change zone. At the peak of phase change, specific heat capacity (combination of latent heat of phase change and sensible heat) can reach 252 % of the reference sample value (when 10 % of PCM is added).

Then, numerical simulations have been undertaken in order to estimate energy savings in a typical single-family home with external vertical walls made of cob-PCM mixtures. Calculations are based on the material's properties obtained experimentally in present work. Results showed an energy saving approaching 13 % for the heating/cooling needs, when cob contains 10 % of Micronal DS 5038 X. However, this study indicated that PCM melting/solidification temperature ranging between 18 °C and 20 °C are more adapted to Caen's climate. With an appropriate phase change temperature (as example 18 °C), the energy gain on heating/cooling needs could approach 30 %.

In the continuity of this work, a validation of the numerical simulation on a large-scale cell will be carried out.

Finally, Micronal DS 5038 X is more expensive than soil or vegetal fibers. Thus, it is highly probable that its introduction into cob will increase the cost of this latter. Consequently, the following question is worth asking: Does the savings due to reduced consumption generated by PCMs remain interesting in view of the additional cost generated by the incorporation of this material?

Acknowledgements

The authors wish to thank Jean-François Bardeau (IMMM, Le Mans Université, France) for the Cp measurement, also Malo Le Guern (ESITC Caen, France) and François Streiff (PnrMCB, France) for the raw materials supply.

References

[1] The Intergovernmental Panel on Climate Change (IPCC), (2018). https://www.ipcc.ch/languages-2/francais/ (accessed September 1, 2021).
[2] Atmospheric greenhouse gas concentrations — European Environment Agency, (2018). https://www.eea.europa.eu/data-and-maps/indicators/atmospheric-greenhouse-gas-concentrations-7/assessment (accessed September 1, 2021).
[3] Émissions de gaz à effet de serre par activité | Insee, (2021). https://www.insee.fr/fr/statistiques/2015759#graphique-figure1 (accessed October 21, 2021).
[4] Commissariat général au développement durable, Chiffres Clés Clim. (2021). https://www.statistiques.developpement-durable.gouv.fr/ (accessed October 21, 2021).
[5] E. Hache, D. Leboullenger, V. Mignon, Beyond average energy consumption in the French residential housing market: A household classification approach, Energy Policy. 107 (2017) 82–95. https://doi.org/10.1016/j.enpol.2017.04.038.
[6] A. Toleikyte, L. Kranzl, A. Müller, Cost curves of energy efficiency investments in buildings – Methodologies and a case study of Lithuania, Energy Policy. 115 (2018) 148–157. https://doi.org/10.1016/j.enpol.2017.12.043.
[7] S. Thomas, J. Thema, M. Kopatz, Energy sufficiency policy: how to limit energy consumption and per capita dwelling size in a decent way, (2017) 10.
[8] N. Sebaibi, M. Boutouil, Reducing energy consumption of prefabricated building elements and lowering the environmental impact of concrete, Eng. Struct. 213 (2020) 110594. https://doi.org/10.1016/j.engstruct.2020.110594.
[9] L. Wells, B. Rismanchi, L. Aye, A review of Net Zero Energy Buildings with reflections on the Australian context, Energy Build. 158 (2018) 616–628. https://doi.org/10.1016/j.enbuild.2017.10.055.
[10] L.F. Cabeza, C. Barreneche, L. Miró, M. Martínez, A.I. Fernández, D. Urge-Vorsatz, Affordable construction towards sustainable buildings: review on embodied energy in building materials, Curr. Opin. Environ. Sustain. 5 (2013) 229–236. https://doi.org/10.1016/j.cosust.2013.05.005.
[11] T.H. Oliver, M.D. Morecroft, Interactions between climate change and land use change on biodiversity: attribution problems, risks, and opportunities, WIREs Clim. Change. 5 (2014) 317–335. https://doi.org/10.1002/wcc.271.
[12] A. Koezjakov, D. Urge-Vorsatz, W. Crijns-Graus, M. van den Broek, The relationship between operational energy demand and embodied energy in Dutch residential buildings, Energy Build. 165 (2018) 233–245. https://doi.org/10.1016/j.enbuild.2018.01.036.
[13] A. Lupíšek, M. Vaculíková, Š. ManĽík, J. Hodková, J. RůžiĽka, Design Strategies for Low Embodied Carbon and Low Embodied Energy Buildings: Principles and Examples, Energy Procedia. 83 (2015) 147–156. https://doi.org/10.1016/j.egypro.2015.12.205.
[14] H. Bui, N. Sebaibi, M. Boutouil, D. Levacher, Determination and Review of Physical and Mechanical Properties of Raw and Treated Coconut Fibers for Their Recycling in Construction Materials, Fibers. 8 (2020) 37. https://doi.org/10.3390/fib8060037.
[15] United Nations Environment Programme, The Emissions Gap Report 2017: A UN Environment Synthesis Report, UN, 2017. https://doi.org/10.18356/1cf881fb-en.
[16] G. Semprini, R. Gulli, A. Ferrante, Deep regeneration vs shallow renovation to achieve nearly Zero Energy in existing buildings: Energy saving and economic impact of design solutions in the housing stock of Bologna, Energy Build. 156 (2017) 327–342. https://doi.org/10.1016/j.enbuild.2017.09.044.
[17] A. Brambilla, G. Salvalai, M. Imperadori, M.M. Sesana, Nearly zero energy building renovation: From energy efficiency to environmental efficiency, a pilot case study, Energy Build. 166 (2018) 271–283. https://doi.org/10.1016/j.enbuild.2018.02.002.

[18] D. D'Agostino, D. Parker, A framework for the cost-optimal design of nearly zero energy buildings (NZEBs) in representative climates across Europe, Energy. 149 (2018) 814–829. https://doi.org/10.1016/j.energy.2018.02.020.
[19] K. Ruiwen, Properties of high-strength foam concrete, Master thesis, National University of Singapore, 2004. https://scholarbank.nus.edu.sg/handle/10635/27683 (accessed November 25, 2020).
[20] T.S. Yun, Y.J. Jeong, T.-S. Han, K.-S. Youm, Evaluation of thermal conductivity for thermally insulated concretes, Energy Build. 61 (2013) 125–132. https://doi.org/10.1016/j.enbuild.2013.01.043.
[21] L.H. Nguyen, A.-L. Beaucour, S. Ortola, A. Noumowé, Influence of the volume fraction and the nature of fine lightweight aggregates on the thermal and mechanical properties of structural concrete, Constr. Build. Mater. 51 (2014) 121–132. https://doi.org/10.1016/j.conbuildmat.2013.11.019.
[22] P.C. Chidighikaobi, Thermal effect on the flexural strength of expanded clay lightweight basalt fiber reinforced concrete, Mater. Today Proc. 19 (2019) 2467–2470. https://doi.org/10.1016/j.matpr.2019.08.110.
[23] H. Karaky, C. Maalouf, C. Bliard, T. Moussa, N. El Wakil, M. Lachi, G. Polidori, Hygrothermal and Acoustical Performance of Starch-Beet Pulp Composites for Building Thermal Insulation, Materials. 11 (2018) 1622. https://doi.org/10.3390/ma11091622.
[24] H. Karaky, C. Maalouf, C. Bliard, A. Gacoin, M. Lachi, N. El Wakil, G. Polidori, Characterization of beet-pulp fiber reinforced potato starch biopolymer composites for building applications, Constr. Build. Mater. 203 (2019) 711–721. https://doi.org/10.1016/j.conbuildmat.2019.01.127.
[25] A. Bourdot, T. Moussa, A. Gacoin, C. Maalouf, P. Vazquez, C. Thomachot-Schneider, C. Bliard, A. Merabtine, M. Lachi, O. Douzane, H. Karaky, G. Polidori, Characterization of a hemp-based agro-material: Influence of starch ratio and hemp shive size on physical, mechanical, and hygrothermal properties, Energy Build. 153 (2017) 501–512. https://doi.org/10.1016/j.enbuild.2017.08.022.
[26] T. Colinart, T. Vinceslas, H. Lenormand, A.H.D. Menibus, E. Hamard, T. Lecompte, Hygrothermal properties of light-earth building materials, J. Build. Eng. 29 (2020) 101134. https://doi.org/10.1016/j.jobe.2019.101134.
[27] A. Laborel-Préneron, J.E. Aubert, C. Magniont, C. Tribout, A. Bertron, Plant aggregates and fibers in earth construction materials: A review, Constr. Build. Mater. 111 (2016) 719–734. https://doi.org/10.1016/j.conbuildmat.2016.02.119.
[28] K. Holzhueter, K. Itonaga, The Potential for Light Straw Clay Construction in Japan: An Examination of the Building Method and Thermal Performance, J. Asian Archit. Build. Eng. 16 (2017) 209–213. https://doi.org/10.3130/jaabe.16.209.
[29] T.A. Phung, Formulation et caractérisation d'un composite terre-fibres végétales: la bauge, PhD Thesis, Normandie Université, 2018. https://tel.archives-ouvertes.fr/tel-01938827 (accessed January 5, 2021).
[30] E. Hamard, Rediscovering of vernacular adaptative construction strategies for sustainable modern building : application to cob and rammed earth, Université de Lyon, 2017. https://www.researchgate.net/publication/323387530_Rediscovering_of_vernacular_adaptative_construction_strategies_for_sustainable_modern_building_application_to_cob_and_rammed_earth.
[31] S. Goodhew, J. Carfrae, K. Hood-Cree, M. Fox, M. Boutouil, F. Streiff, Building with earth: How we are working to revive an ancient, sustainable building technique, Constr. Res. Innov. 10 (2019) 105–108. https://doi.org/10.1080/20450249.2019.1700077.
[32] F. Alassaad, K. Touati, D. Levacher, N. Sebaibi, Impact of phase change materials on lightened earth hygroscopic, thermal and mechanical properties, J. Build. Eng. 41 (2021) 102417. https://doi.org/10.1016/j.jobe.2021.102417.
[33] M. Bouasria, Y. El Mendili, M.-H. Benzaama, V. Pralong, J.-F. Bardeau, F. Hennequart, Valorisation of stranded Laminaria digitata seaweed as an insulating earth material, Constr. Build. Mater. 308 (2021) 125068. https://doi.org/10.1016/j.conbuildmat.2021.125068.

[34] A. Azil, M. Le Guern, K. Touati, N. Sebaibi, M. Boutouil, F. Streiff, S. Goodhew, M. Gomina, Earth construction: Field variabilities and laboratory reproducibility, Constr. Build. Mater. 314 (2022) 125591. https://doi.org/10.1016/j.conbuildmat.2021.125591.
[35] Cob Houses Are the Ultimate Eco-Friendly Homes—Here's 5 You Can Visit, Brightly. (2021). https://brightly.eco/cob-houses/ (accessed January 24, 2022).
[36] Cob Homes around the World, (n.d.). http://naturalhomes.org/natural-building-cob.htm (accessed January 24, 2022).
[37] L. Dipasquale, Correia, M., Dipasquale, L., Mecca, S. (eds.), Terra Europae, Earthen Architecture in the European Union, ETS, Pisa, pp.216., (2011). https://www.academia.edu/4440548/Correia_M_Dipasquale_L_Mecca_S_eds_Terra_Europae_Earthen_Architecture_in_the_European_Union_ETS_Pisa_2011_pp_216 (accessed January 13, 2022).
[38] L. Zhang, G. Sang, W. Han, Effect of hygrothermal behaviour of earth brick on indoor environment in a desert climate, Sustain. Cities Soc. 55 (2020) 102070. https://doi.org/10.1016/j.scs.2020.102070.
[39] H. Cagnon, J.E. Aubert, M. Coutand, C. Magniont, Hygrothermal properties of earth bricks, Energy Build. 80 (2014) 208–217. https://doi.org/10.1016/j.enbuild.2014.05.024.
[40] D. Medjelekh, L. Ulmet, F. Dubois, Characterization of hygrothermal transfers in the unfired earth, Energy Procedia. 139 (2017) 487–492. https://doi.org/10.1016/j.egypro.2017.11.242.
[41] P.M. Touré, V. Sambou, M. Faye, A. Thiam, M. Adj, D. Azilinon, Mechanical and hygrothermal properties of compressed stabilized earth bricks (CSEB), J. Build. Eng. 13 (2017) 266–271. https://doi.org/10.1016/j.jobe.2017.08.012.
[42] G. Giuffrida, R. Caponetto, F. Nocera, Hygrothermal Properties of Raw Earth Materials: A Literature Review, Sustainability. (2019). https://doi.org/10.3390/su11195342.
[43] R. Anger, L. Fontaine, T. Joffroy, E. Ruiz, Construire en terre, une autre voie pour loger la planète, Sect. Privé Dév. Rev. Bimest. Proparco. 10 (2011) 18–21.
[44] A. Azil, M. le guern, K. Touati, M. Gomina, N. Sebaibi, F. Streiff, S. Goodhew, H. Louahlia, CONSTRUCTION FIELD MONITORING OF A COB PROTOTYPE BUILDING, in: 2021.
[45] R. Nabouch, Q.B. Bui, O. Plé, P. Perrotin, C. Poinard, T. Goldin, J.P. Plassiard, Seismic Assessment of Rammed Earth Walls Using Pushover Tests, Procedia Eng. 145 (2016) 1185–1192. https://doi.org/10.1016/j.proeng.2016.04.153.
[46] T.A. Phung, M. Le Guern, M. Boutouil, H. Louahlia, Hygrothermal Behaviour of Cob Material, in: B.V.V. Reddy, M. Mani, P. Walker (Eds.), Earthen Dwell. Struct., Springer Singapore, Singapore, 2019: pp. 345–356. https://doi.org/10.1007/978-981-13-5883-8_30.
[47] I. Niang, C. Maalouf, T. Moussa, C. Bliard, E. Samin, C. Thomachot-Schneider, M. Lachi, H. Pron, T.H. Mai, S. Gaye, Hygrothermal performance of various Typha–clay composite, J. Build. Phys. 42 (2018) 316–335. https://doi.org/10.1177/1744259118759677.
[48] M. Labat, C. Magniont, N. Oudhof, J.-E. Aubert, From the experimental characterization of the hygrothermal properties of straw-clay mixtures to the numerical assessment of their buffering potential, Build. Environ. 97 (2016) 69–81. https://doi.org/10.1016/j.buildenv.2015.12.004.
[49] ADEME, feuille de route stratégique sur les systèmes de stockage d'énergie, (2011). http://www.ademe.fr/sites/default/files/assets/documents/6919_stockageenergie.pdf.
[50] N. Soares, J.J. Costa, A.R. Gaspar, P. Santos, Review of passive PCM latent heat thermal energy storage systems towards buildings' energy efficiency, Energy Build. 59 (2013) 82–103. https://doi.org/10.1016/j.enbuild.2012.12.042.
[51] P. Devaux, M.M. Farid, Benefits of PCM underfloor heating with PCM wallboards for space heating in winter, Appl. Energy. 191 (2017) 593–602. https://doi.org/10.1016/j.apenergy.2017.01.060.
[52] Faculty of Arts and Sciences, Department of Chemistry, Cukurova University, 01330, Saricam Adana, Turkey, K. Cellat, B. Beyhan, B. Kazanci, Y. Konuklu, H. Paksoy, Direct Incorporation of Butyl Stearate as Phase Change Material into Concrete for Energy Saving in Buildings, J. Clean Energy Technol. 5 (2017) 64–68. https://doi.org/10.18178/JOCET.2017.5.1.345.
[53] S. Cunha, P. Leite, J. Aguiar, Characterization of innovative mortars with direct incorporation of phase change materials, J. Energy Storage. 30 (2020) 101439. https://doi.org/10.1016/j.est.2020.101439.

[54] S. Cunha, M. Lima, J.B. Aguiar, Influence of adding phase change materials on the physical and mechanical properties of cement mortars, Constr. Build. Mater. 127 (2016) 1–10. https://doi.org/10.1016/j.conbuildmat.2016.09.119.
[55] D.W. Hawes, D. Feldman, Absorption of phase change materials in concrete, Sol. Energy Mater. Sol. Cells. 27 (1992) 91–101. https://doi.org/10.1016/0927-0248(92)90112-3.
[56] H. Kaasinen, The absorption of phase change substances into commonly used building materials, Sol. Energy Mater. Sol. Cells. 27 (1992) 173–179. https://doi.org/10.1016/0927-0248(92)90118-9.
[57] L.F. Cabeza, C. Castellón, M. Nogués, M. Medrano, R. Leppers, O. Zubillaga, Use of microencapsulated PCM in concrete walls for energy savings, Energy Build. 39 (2007) 113–119. https://doi.org/10.1016/j.enbuild.2006.03.030.
[58] V.D. Cao, S. Pilehvar, C. Salas-Bringas, A.M. Szczotok, J.F. Rodriguez, M. Carmona, N. Al-Manasir, A.-L. Kjøniksen, Microencapsulated phase change materials for enhancing the thermal performance of Portland cement concrete and geopolymer concrete for passive building applications, Energy Convers. Manag. 133 (2017) 56–66. https://doi.org/10.1016/j.enconman.2016.11.061.
[59] C. Castellón, M. Medrano, A. Castell, J. Roca, L.F. Cabeza, M. Nogués, Use of Microencapsulated Phase Change Materials in Building Applications, (2006) 6.
[60] E. Franquet, S. Gibout, P. Tittelein, L. Zalewski, J.-P. Dumas, Experimental and theoretical analysis of a cement mortar containing microencapsulated PCM, Appl. Therm. Eng. 73 (2014) 32–40. https://doi.org/10.1016/j.applthermaleng.2014.06.053.
[61] P.K.S. Rathore, S.K. Shukla, Potential of macroencapsulated PCM for thermal energy storage in buildings: A comprehensive review, Constr. Build. Mater. 225 (2019) 723–744. https://doi.org/10.1016/j.conbuildmat.2019.07.221.
[62] M. Gandhi, A. Kumar, R. Elangovan, C.S. Meena, K.S. Kulkarni, A. Kumar, G. Bhanot, N.R. Kapoor, A Review on Shape-Stabilized Phase Change Materials for Latent Energy Storage in Buildings, Sustainability. 12 (2020) 9481. https://doi.org/10.3390/su12229481.
[63] W. Cheng, B. Xie, R. Zhang, Z. Xu, Y. Xia, Effect of thermal conductivities of shape stabilized PCM on under-floor heating system, Appl. Energy. 144 (2015) 10–18. https://doi.org/10.1016/j.apenergy.2015.01.055.
[64] H. Inaba, P. Tu, Evaluation of thermophysical characteristics on shape-stabilized paraffin as a solid-liquid phase change material, Heat Mass Transf. 32 (1997) 307–312. https://doi.org/10.1007/s002310050126.
[65] S. Ramakrishnan, J. Sanjayan, X. Wang, Experimental Research on Using Form-stable PCM-Integrated Cementitious Composite for Reducing Overheating in Buildings, Buildings. 9 (2019) 57. https://doi.org/10.3390/buildings9030057.
[66] Z. Zhang, G. Alva, M. Gu, G. Fang, Experimental investigation on n–octadecane/polystyrene/expanded graphite composites as form–stable thermal energy storage materials, Energy. 157 (2018) 625–632. https://doi.org/10.1016/j.energy.2018.06.006.
[67] C. Reuben Raj, S. Suresh, S. Vasudevan, M. Chandrasekar, V. Kumar Singh, R.R. Bhavsar, Thermal performance of nano-enriched form-stable PCM implanted in a pin finned wall-less heat sink for thermal management application, Energy Convers. Manag. 226 (2020) 113466. https://doi.org/10.1016/j.enconman.2020.113466.
[68] A. Sarı, A. Karaipekli, Preparation, thermal properties and thermal reliability of capric acid/expanded perlite composite for thermal energy storage, Mater. Chem. Phys. 109 (2008) 459–464. https://doi.org/10.1016/j.matchemphys.2007.12.016.
[69] A. Sarı, Form-stable paraffin/high density polyethylene composites as solid–liquid phase change material for thermal energy storage: preparation and thermal properties, Energy Convers. Manag. 45 (2004) 2033–2042. https://doi.org/10.1016/j.enconman.2003.10.022.
[70] A. Karaipekli, A. Sarı, Capric–myristic acid/vermiculite composite as form-stable phase change material for thermal energy storage, Sol. Energy. 83 (2009) 323–332. https://doi.org/10.1016/j.solener.2008.08.012.
[71] S. Karaman, A. Karaipekli, A. Sarı, A. Biçer, Polyethylene glycol (PEG)/diatomite composite as a novel form-stable phase change material for thermal energy storage, Sol. Energy Mater. Sol. Cells. 95 (2011) 1647–1653. https://doi.org/10.1016/j.solmat.2011.01.022.

[72] X. Fang, P. Hao, B. Song, C.-C. Tuan, C.-P. Wong, Z.-T. Yu, Form-stable phase change material embedded with chitosan-derived carbon aerogel, Mater. Lett. 195 (2017) 79–81. https://doi.org/10.1016/j.matlet.2017.02.075.
[73] S. Cunha, J. Aguiar, F. Pacheco-Torgal, Effect of temperature on mortars with incorporation of phase change materials, Constr. Build. Mater. 98 (2015) 89–101. https://doi.org/10.1016/j.conbuildmat.2015.08.077.
[74] Z. Dakhli, K. Chaffar, Z. Lafhaj, The Effect of Phase Change Materials on the Physical, Thermal and Mechanical Properties of Cement, Sci. 1 (2019) 27. https://doi.org/10.3390/sci1010027.
[75] Z.I. Djamai, F. Salvatore, A. Si Larbi, G. Cai, M. El Mankibi, Multiphysics analysis of effects of encapsulated phase change materials (PCMs) in cement mortars, Cem. Concr. Res. 119 (2019) 51–63. https://doi.org/10.1016/j.cemconres.2019.02.002.
[76] S. Drissi, A. Eddhahak, J. Neji, S. Caré, Etude de l'impact des Matériaux à Changement de Phase (MCP) sur l'hydratation des bétons-MCP, Conférence Journ. Sci. Fr.-Maghrébines-CMC Tunis. (2014) 6.
[77] S.Y. Kong, Z.H. See, C.L. Lee, X. Yang, L.S. Wong, T.S. Goh, Thermal and mechanical properties of mortar incorporated with paraffin/palm oil fuel ash composite, J. Build. Eng. 26 (2019) 100923. https://doi.org/10.1016/j.jobe.2019.100923.
[78] S. Cunha, J. Aguiar, V. Ferreira, A. Tadeu, Mortars based in different binders with incorporation of phase-change materials: Physical and mechanical properties, Eur. J. Environ. Civ. Eng. 19 (2015) 1216–1233. https://doi.org/10.1080/19648189.2015.1008651.
[79] T.-C. Ling, C.-S. Poon, Use of phase change materials for thermal energy storage in concrete: An overview, Constr. Build. Mater. 46 (2013) 55–62. https://doi.org/10.1016/j.conbuildmat.2013.04.031.
[80] S. Serrano, C. Barreneche, L. Rincón, D. Boer, L.F. Cabeza, Stabilized rammed earth incorporating PCM: Optimization and improvement of thermal properties and Life Cycle Assessment, Energy Procedia. 30 (2012) 461–470. https://doi.org/10.1016/j.egypro.2012.11.055.
[81] M. Delgado, I. Cañas, The selection of soils for unstabilised earth building: A normative review, Constr. Build. Mater. 21 (2007) 237–251. https://doi.org/10.1016/j.conbuildmat.2005.08.006.
[82] XP P94-041, Soil : investigation and testing. Granulometric description. Wet sieving method., XP P94-041, 1995. https://sagaweb.afnor.org.
[83] NF EN ISO 17892-12, Geotechnical investigation and testing - Laboratory testing of soil - Part 12 : determination of liquid and plastic limits, NF EN ISO 17892-12, 2018. https://cobaz.afnor.org/notice/norme/nf-en-iso-17892-12/FA187930?rechercheID=4973543&searchIndex=1&activeTab=all#id_lang_2_Titles (accessed January 25, 2022).
[84] NF P94-068, Soils : investigation and testing. Measuring of the methylene blue adsorption capacity of à rocky soil. Determination of the methylene blue of a soil by means of the stain test., NF P94-068, 1998. https://sagaweb.afnor.org.
[85] ASTM D2487-06, Standard Practice for Classification of Soils for Engineering Purposes (Unified Soil Classification System), ASTM D2487-06, 2010. https://www.astm.org/d2487-06.html (accessed January 26, 2022).
[86] S. Gražulis, A. Daškevič, A. Merkys, D. Chateigner, L. Lutterotti, M. Quirós, N.R. Serebryanaya, P. Moeck, R.T. Downs, A. Le Bail, Crystallography Open Database (COD): an open-access collection of crystal structures and platform for world-wide collaboration, Nucleic Acids Res. 40 (2012) D420-427. https://doi.org/10.1093/nar/gkr900.
[87] L. Lutterotti, S. Matthies, H.-R. Wenk, A.S. Schultz, J.W. Richardson, Combined texture and structure analysis of deformed limestone from time-of-flight neutron diffraction spectra, J. Appl. Phys. 81 (1997) 594–600. https://doi.org/10.1063/1.364220.
[88] D. Hillel, 5. - SOIL PHYSICAL ATTRIBUTES, in: D. Hillel (Ed.), Soil Environ., Academic Press, San Diego, 2008: pp. 55–77. https://doi.org/10.1016/B978-0-12-348536-6.50010-1.
[89] Météo France, (2019). http://www.meteofrance.fr/climat-passe-et-futur/bilans-climatiques/bilan-2019/bilan-climatique-de-l-ete-2019# (accessed October 21, 2020).
[90] A. Sarı, A. Karaipekli, K. Kaygusuz, Capric acid and stearic acid mixture impregnated with gypsum wallboard for low-temperature latent heat thermal energy storage, Int. J. Energy Res. 32 (2008) 154–160. https://doi.org/10.1002/er.1352.

[91] S. Park, Y. Lee, Y.S. Kim, H.M. Lee, J.H. Kim, I.W. Cheong, W.-G. Koh, Magnetic nanoparticle-embedded PCM nanocapsules based on paraffin core and polyurea shell, Colloids Surf. Physicochem. Eng. Asp. 450 (2014) 46–51. https://doi.org/10.1016/j.colsurfa.2014.03.005.
[92] C. Group, Microtek Laboratories, (2020). https://www.microteklabs.com (accessed October 22, 2020).
[93] S. Drissi, Développement de nouveaux bétons "'accumulateurs d'énergie'": investigations expérimentale, probabiliste et numérique du comportement thermique, phd, l'Ecole Nationale d'Ingénieurs de Tunis et l'Université Paris-EST, 2015. https://pastel.archives-ouvertes.fr/tel-01271597/document (accessed November 15, 2019).
[94] NF EN 1015-11, Methods of test for mortar for masonry - Part 11 : determination of flexural and compressive strength of hardened mortar, NF EN 1015-11, 2019. https://sagaweb.afnor.org.
[95] NF EN ISO 12572, Hygrothermal performance of building materials and products - Determination of water vapour transmission properties - Cup method, NF EN ISO 12572, 2016. https://sagaweb.afnor.org.
[96] NF EN ISO 12571, Hygrothermal performance of building materials and products - Determination of hygroscopic sorption properties, NF EN ISO 12571, 2013. https://sagaweb.afnor.org.
[97] J.W. Gooch, Fourier's Law of Heat Conduction, in: J.W. Gooch (Ed.), Encycl. Dict. Polym., Springer, New York, NY, 2011: pp. 323–323. https://doi.org/10.1007/978-1-4419-6247-8_5262.
[98] Plastiques — Analyse calorimétrique différentielle (DSC) — Partie 4 : Détermination de la capacité thermique massique, NF EN ISO 11357-4, 2014. https://sagaweb.afnor.org/.
[99] R. Harries, B. Saxton, K. Coventry, The geological and geotechnical properties of earth material from, in: 1995.
[100] O. Akinkurolere, Cangru Jiang, A.T. Oyediran, O.I. Dele-Salawu, A.K. Elensinnla, Engineering Properties of Cob as a Building Material, J. Appl. Sci. 6: 1882-1885 (2006). https://doi.org/10.3923/jas.2006.1882.1885.
[101] E. Quagliarini, G. Maracchini, Experimental and FEM Investigation of Cob Walls under Compression, Adv. Civ. Eng. 2018 (2018) e7027432. https://doi.org/10.1155/2018/7027432.
[102] L. Miccoli, U. Müller, P. Fontana, Mechanical behaviour of earthen materials: A comparison between earth block masonry, rammed earth and cob, Constr. Build. Mater. 61 (2014) 327–339. https://doi.org/10.1016/j.conbuildmat.2014.03.009.
[103] J.-P. Oliva, S.C. Courgey, L'isolation thermique écologique. Conception, matériaux, mise en oeuvre, 2001.
[104] F. Stazi, A. Nacci, F. Tittarelli, E. Pasqualini, P. Munafò, An experimental study on earth plasters for earthen building protection: The effects of different admixtures and surface treatments, J. Cult. Herit. 17 (2016) 27–41. https://doi.org/10.1016/j.culher.2015.07.009.
[105] F. Collet-Foucault, Caractérisation hydrique et thermique de matériaux de génie civil à faibles impacts environnementaux, These de doctorat, Rennes, INSA, 2004. http://www.theses.fr/2004ISAR0016 (accessed November 26, 2020).
[106] N. Issaadi, A. Nouviaire, R. Belarbi, A. Aït-Mokhtar, Moisture characterization of cementitious material properties: Assessment of water vapor sorption isotherm and permeability variation with ages, Constr. Build. Mater. 83 (2015) 237–247. https://doi.org/10.1016/j.conbuildmat.2015.03.030.